ORIGINAL ARTICLE

ANDROLOGY WILEY

Rapid detection of mouse spermatogenic defects by testicular cellular composition analysis via enhanced deep learning model

Nianfei Ao[1] | Min Zang[2] | Yue Lu[2] | Yiping Jiao[1] | Haoda Lu[1,3] | Chengfei Cai[1] |
Xiangxue Wang[1] | Xin Li[2] | Minge Xie[4] | Tingting Zhao[2] | Jun Xu[1] |
Eugene Yujun Xu[2,5,6] (iD)

[1]Jiangsu Key Laboratory of Intelligent Medical Image Computing, School of Artificial Intelligence, Nanjing University of Information Science and Technology, Nanjing, Jiangsu, China

[2]State Key Laboratory of Reproductive Medicine and Offspring Health, Nanjing Medical University, Nanjing, Jiangsu, China

[3]Bioinformatics Institute, A*STAR, Singapore, Singapore

[4]Department of Statistics, Rutgers University, Piscataway, New Jersey, USA

[5]Cellular Screening Center (RRID:SCR_017914), The University of Chicago, Chicago, Illinois, USA

[6]Department of Neurology, Center for Reproductive Sciences, Northwestern University Feinberg School of Medicine, Chicago, Illinois, USA

Correspondence
Tingting Zhao, State Key Laboratory of Reproductive Medicine and Offspring Health, Nanjing Medical University, Nanjing, Jiangsu, 210029, China.
Email: zhaotiti@njmu.edu.cn

Jun Xu, Jiangsu Key Laboratory of Intelligent Medical Image Computing, School of Artificial Intelligence, Nanjing University of Information Science and Technology, Nanjing, 210044, China.
Email: jxu@nuist.edu.cn

Eugene Yujun Xu, Cellular Screening Center, The University of Chicago, Chicago, IL 60637, USA.
Email: yxu@uchicago.edu

Abstract

Background: Histological analysis of the testicular sections is paramount in infertility research but tedious and often requires months of training and practice.

Objectives: Establish an expeditious histopathological analysis of mutant mice testicular sections stained with commonly available hematoxylin and eosin (H&E) via enhanced deep learning model

Materials and Methods: Automated segmentation and cellular composition analysis on the testes of six mouse reproductive mutants of key reproductive gene family, *DAZ* and *PUMILIO* gene family via H&E-stained mouse testicular sections.

Results: We improved the deep learning model with human interaction to achieve better pixel accuracy and reduced annotation time for histologists; revealed distinctive cell composition features consistent with previously published phenotypes for four mutants and novel spermatogenic defects in two newly generated mutants; established a fast spermatogenic defect detection protocol for quantitative and qualitative assessment of testicular defects within 2.5–3 h, requiring as few as 8 H&E-stained testis sections; uncovered novel defects in AcDKO and a meiotic arrest defect in HDBKO, supporting the synergistic interaction of Sertoli *Pum1* and *Pum2* as well as redundant meiotic function of *Dazl* and *Boule*.

Nianfei Ao and Min Zang contributed equally to this work.

- -

Discussion: Our testicular compositional analysis not only could reveal spermatogenic defects from staged seminiferous tubules but also from unstaged seminiferous tubule sections.

Conclusion: Our SCSD-Net model offers a rapid protocol for detecting reproductive defects from H&E-stained testicular sections in as few as 3 h, providing both quantitative and qualitative assessments of spermatogenic defects. Our analysis uncovered evidence supporting the synergistic interaction of Sertoli PUM1 and PUM2 in maintaining average testis size, and redundant roles of *DAZ* family proteins DAZL and BOULE in meiosis.

KEYWORDS
BOULE, DAZL, deep learning, PUMILIO, seminiferous tubules testis histology

1 | INTRODUCTION

The development of spermatozoa is a complex, continuous reproductive process in mammals, resulting in constant sperm production. However, defects in human spermatogenesis may lead to infertility, affecting approximately 15% of couples worldwide and up to 7% of males of reproductive age.[1–3] A major contributor to male infertility is the absence of spermatozoon or abnormalities in sperm morphology and motility. Given the similarity between the mouse and human reproductive systems, mouse knockout and transgenic models that result in male sterility have become excellent model systems for understanding the genetic basis of human infertility.[4] The phenotypic analysis of infertile mouse testes is crucial for understanding spermatogenesis defects, especially by histopathological examination. The process of sperm development begins with spermatogonia, which undergoes mitosis to increase in number and then becomes spermatocytes to complete meiotic divisions, transition through round spermatids, elongated spermatids, and ultimately culminates in the formation of mature sperm. These germ cells persist in the seminiferous tubules of the testis, constituting the fundamental units of spermatogenesis.[5–7] Systematic methods for manual characterization of the testis exist in the laboratory context, including Russel et al.[8] evaluating the testis in a toxicological testing environment and a more comprehensive approach proposed by McLachlan et al.[9] to histologically classify spermatogenetic disorders and carcinoma in situ in adult patients. However, manual assessment of testicular cross-sections is time consuming and laborious due to the typically high pixel density of whole slide images (WSIs). In addition, differences in processing protocols, tissue preparation methods, training levels, and histologist experience often contribute to increased inter- and intra-observer variability. Therefore, the development of automated classification methods for testicular histopathology is necessary to address the quantitative analysis of testicular tissues of infertile mice, particularly for accurate analysis of cellular composition during the spermatogenesis stage.

While the quality of testicular histology has improved significantly over the past decade, computer-aided tools for processing and analyzing such data are slowly emerging.[10,11] The recent development of neural networks and deep learning accelerated the growth in the field. They led to several studies developing automated or semi-automated staging of testis histology and classification of testicular cell types in animals and humans.[12–17] To understand testicular histology or pathology, performing correct staging of the testis sections is essential before analyzing the testicular cell types. It is even more critical in analyzing mutant testis phenotypes via staging. Furthermore, epithelial cycles, the number of stages per cycle, and the arrangement of different spermatogenic cell types often differ among other animals and humans.[5,8] Even mice and rats are different, with 12 epithelial stages for mice and 14 for rats, necessitating the development of a species-specific staging automation system.

We have been developing a computerized automated staging system (CSS) for hematoxylin and eosin (H&E)-stained mouse testis sections.[14,18,19] Ghoshal et al.[20] presented DeepHistoClass, a method automating the classification of testicular immunohistochemical images, providing model confidence outputs simultaneously. Dumont et al.[13] developed an open-source Fiji program for quantitatively assessing testicular tissue slices. However, despite these advancements, identifying aberrant testicular cells and spermatogenic defects during development remains challenging, and current research is still in the exploratory stage. Ito et al.[16] utilized a public Google Cloud system to develop an automated evaluation of human testicular cells from infertile men. Bell et al.[21] described an automated identification method of multinucleated germ cells in rat testes induced by reproductive toxicants using U-Net. Recently, Yang et al.[15] and Meikar et al.[17] developed fluorescent labeling-based automated methods for mouse testicular staging and cell type identification and applied their software to the staging of mutant mice. While fluorescently labeled testis sections provided more distinctive features of spermatogenic cells, allowing the identification of more stage categories and cell type categories than bright field testis sections, H&E staining technology remains the most common histology methodology and is routinely available for the analysis of the testis sections in the reproductive biology lab and hospitals. A deep learning model detecting and identifying

WILEY | 3

testicular defects in the infertile mutant mice or toxicant-exposed mice from the H&E-stained section may have a wide application. We further improved automatic CSS using a multiscale learning model and reported a novel segmentation model for the automatic segmentation of testicular cells using H&E-stained testicular sections,[14,18,19] but all the work has been based on wild-type testis with normal spermatogenesis including the training dataset from wild-type testes, making it challenging to generalize their broad application to unknown mutant phenotypes. Significant increases in apoptotic spermatogenic cells and disorganization of cellular arrangement due to disruption of spermatogenesis in mutant mice are common features of mutant testes. They could impact the precision of automated analysis based on the wild-type testis training model.

Developing an automated system using mutant testis in training could address this issue and lead to broad application in the histopathology analysis of mutant testes. Additionally, while nuanced analysis of cells can be achieved through immunofluorescence, its cost compared with histopathology remains significantly high, limiting its application in large-scale studies. In contrast, H&E staining is an inexpensive and routine testis histology method; however, existing approaches face challenges in achieving high-precision cell classification due to cellular morphological similarities on H&E-stained slides.

Deep learning is an effective method for distinguishing subtle differences in tissue morphology. Still, establishing models require substantial annotated data, which are time consuming and require extensive training for a new histologist. To evaluate the specific impact of spermatogenic disorders, conducting analyses on the cellular level (testicular cell composition proportions and stages recognition) is essential. This specific semantic segmentation requirement presents a considerable challenge for model development. To overcome these challenges, this study introduces an interactive learning approach to achieve efficient "human-in-the loop (HIL)" work,[22] thereby constructing a sufficient quantity of high-quality training datasets. Guo et al.[23,24] have validated the significant effectiveness of interactive learning in enhancing expert knowledge-based medical image analysis through performance evaluations. While interactive learning techniques have been applied in studies on osteosarcoma and gastric cancer.[25,26] Its application and significance in automated testicular histology have not been explored, especially in identifying defects in reproductive mutant testes.

Inspired by these studies, we chose a series of mouse knockout mutants that impacted spermatogenesis quantitatively and qualitatively to systematically explore the feasibility of using a deep learning model to quickly identify reproductive defects in the mutant mice testes. The six mouse reproductive mutants include both whole-body knockout and reproductive cell-specific conditional knockout (BKO, HDKO, HDBKO, AcP1KO, AcP2KO, and AcDKO), which exhibited a global disruption of spermatogenesis leading to no sperm production or normal histology with reduced sperm production, or unknown phenotypes from newly generated mouse mutants (Table 1).

These six gene knockouts targeted members of two critical reproductive gene families, *the DAZ* (*Deleted in Azoospermia*) gene family and the *PUMILIO* family, resulting in two distinct categories of spermatogenic defects (Table 1). While both *DAZ* family and *PUM* family are well recognized for their predominant roles in gametogenesis across diverse animal species,[27,28] they are distinct in their contribution to reproduction in that *DAZ* family members are only expressed in the gonads and have gonad-specific and germ cell-restricted function while *PUM* proteins are expressed in many tissues and both somatic cells and germ cells. While individual members of the mouse *DAZ* family, *Boule* and *Dazl* are required for sperm development, respectively,[28–32] the impact of the loss of both *Dazl* and *Boule* in the testis has not been explored. *Pum1* and *Pum2* in Sertoli cells were shown previously to be required for normal testis weight; removal of Sertoli *Pum1* in the whole-body knockout of *Pum2* was used to reveal the synergistic function of *Pum1* and *Pum2* in Sertoli cells.[33] However, due to the expression of *Pum2* in many other tissues of the mouse, including the hypothalamus and pituitary gland, we could not exclude the systemic effect of loss of *Pum2* on the testis weight and Sertoli cell number using this full-body *Pum2* knockout mouse.[34] Hence, generation of Sertoli cell knockout of both *Pum1* and *Pum2* is needed to address this concern. Both *Dazl* and *Boule* double knockout in spermatocytes and Sertoli cell-specific removal of both *Pum1* and *Pum2* requires careful histological analysis of their testicular defects and careful comparison with the individual mouse knockout of each member. To uncover the synergistic effect of both members in their function during spermatogenesis through histological analysis, we explore the use of a deep learning model for detailed quantitative and qualitative analysis of H&E-stained testicular sections to identify novel reproductive defects and establish a protocol for rapid detection of spermatogenic defects.

The *Boule* gene is the ancient member of the human *DAZ* gene family and is conserved throughout metazoans with restricted expression in gonads with *Boule* knockout exhibiting an apparent global arrest of spermatogenesis phenotype at round spermatids (step 6).[35,36]. Despite the spermatogenesis disruption in the *Boule* mutant testis, it still contains major types of testicular cells segmented in our established model,[18,19] making it an excellent training model to detect spermatogenic defects. We proposed using *Boule* knockout (BKO) as a training model to enhance our previously established model using wild-type testis as a training dataset.

Through quantitative analysis of the testicular cellular composition of data from these mutant mice, we not only have made swift identification of novel reproductive defects of two unpublished genetic mutations disrupting essential reproductive genes as well as their phenotypic differences from those in the single mutant testes of their members of the same gene family. We propose a quantitative analysis of testicular cellular composition via SCSD-Net with interactive learning, representing an effective histopathological protocol for rapid detection of testicular defect based on as few as eight mouse testis H&E sections within a few hours.

The symbols used in this paper are displayed in Table S1 and the information for all the mutant mice used is summarized in Table 1.

TABLE 1 Mutant mice used and their reproductive defects.

| Name | Genotype | Reproductive defect | | Notes |
		Fertility	Spermatogenesis	
BKO	*Boule$^{-/-}$*	Sterile	Round spermatid arrest	Shah et al., 2010; VanGompel and Xu, 2010
HDKO	*Hspa2-cre; Dazl$^{F/-}$*	Sterile	Round sperm arrest	Li et al., 2019
HDBKO	*Hspa2-cre; Dazl$^{F/-}$; Boule$^{-/-}$*	Sterile	Spermatocyte arrest	This work
AcP1KO	*Amh-cre; Pum1$^{F/F}$*	Fertile	Reduced testis size	Zhao et al., 2022
AcP2KO	*Amh-cre; Pum2$^{F/F}$*	Fertile	Reduced testis size	Zhao et al., 2022
AcDKO	*Amh-cre; Pum1$^{F/F}$; Pum2$^{F/F}$*	Fertile	Reduced testis size	This work

2 | RESULTS

2.1 | SCSD-Net with interactive learning reduces annotation time and improves performance

2.1.1 | SCSD-Net with classic deep interactive learning

Our cell composition analysis model, utilizing a deep learning approach, consists of three stages (see Figure 1): Segmentation of testicular cross-sections (the initial stage involves the segmentation of testicular cross-sections of seminiferous tubules), Multi-branch segmentation of testicular cells (the second stage employs the deep SCSD-Net and an interactive learning strategy for the multi-branch segmentation of six types of testicular cells), Component comparison analysis (the final stage comprises the component comparison analysis of the six testis cell types).

Our model was trained using 532 control and 162 mutant seminiferous tubule sections from H&E-stained testis sections from both wild-type ($n = 5$) and mouse *Boule* knockout mutant ($n = 3$; Figure 2). Those seminiferous tubule sections were selected after excluding those that were longitudinal, tangential, or had poor staining or fixation quality. To delineate nuclear boundaries accurately in the testicular cells, we introduced an encoder–decoder-style deep neural network named SCSD-Net. This network incorporates squeeze-and-excitation (SE) modules and attention-dense units (Figure 1A) to enhance segmentation and classification performance. To balance accuracy in recognition and model generalization, we employed a HIL learning strategy (Figure 1B). This iterative human–machine interactive process continued until the model achieved the desired performance. The flow chart for the SCSD-Net architecture is presented in Figure 1, and details of the SCSD-Net model, experimental settings, and datasets are provided in Figures S1 and S2 and the Methods section of Supporting Information.

Given the significant reduction in testicular volume and weight in BKO compared with wild-type mice, the distribution and quantity of spermatogenic cells, such as round spermatids (rs), changed significantly. Many dying round spermatids formed multinucleated cysts (Figure 2). These abnormal cell types and misplaced spermatogenic cells in the mutant mice hinder the correct identification and segmentation of cell types, emphasizing the need to use mutant testis as a training model to enhance the detection of reproductive defects.

To minimize the workload of histologists in annotating a large amount of training data, we adopted the HIL method. Figures 2 and S2 illustrated the seminiferous tubule image segmentation results for wt and BKO mice as well as HDKO, HDBKO, before and after applying HIL. Quantitative and qualitative results indicate that this interactive learning process enhances SCSD-Net's segmentation performance. The initially segmented cell numbers are listed in Table S2. Histologists then corrected the initially segmented cells by supplementing under-segmented cells (Sertoli and spermatogonia), correcting misclassified cells (Sertoli, spermatogonia, early spermatocytes, spermatocytes, and round spermatids), and eliminating over-segmentation (apoptotic rspd, redundant tissue, etc.). As the model improved, the portions requiring correction decreased, and the average annotation time per seminiferous tubule decreased from 20 min to 10 min. Quantitative analysis results with and without deep interactive learning are presented in Table S2 and Figure 2. This strategy reduces the workload for histologists, and the improvement in the performance of SCSD-Net is evident.

2.1.2 | Ablation studies on SCSD-Net and comparison with other models

Ablation experiments were conducted to validate SE-Res and attention-dense units' effectiveness in testicular cell segmentation. Table 2 presents the segmentation performance of SCSD compared with three ablated models for the five types of testicular cells (there is no elongating spermatids in the BKO). Our results demonstrate that the incremental addition of SE-Res units, dense units, and CS blocks on the backbone network effectively enhances the segmentation performance of the model (see Table 2).

Table 2 illustrates that SCSD-Net outperforms other models, particularly in segmenting testicular cells in BKO mice. The mean intersection over union (MIoU) and frequency-weighted intersection over union (FWIoU) reach 0.713 and 0.932, respectively. Additionally, addressing the challenge in detecting spermatogonia (spg) and Sertoli cells (sc), we tested the performance of SCSD-Net (values in bold) on these two challenging cell types. We found it the best, with classification pixel accuracy (CPA) reaching 0.802 and 0.669,
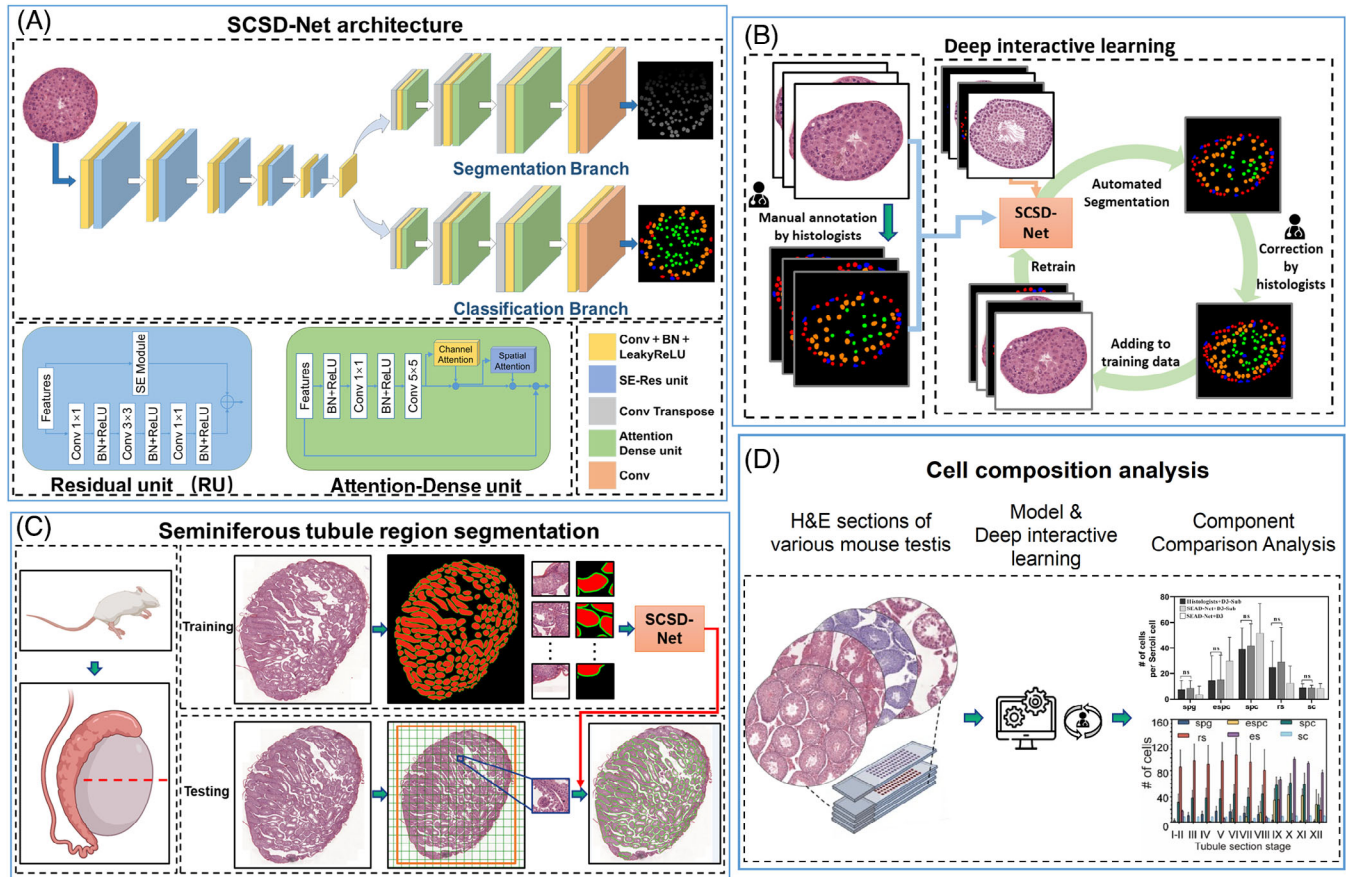
FIGURE 1 Overview of SCSD-Net segmentation. The SCSD-Net architecture (A) comprises cell segmentation and classification branches. Different modules are shown by corresponding colors in (A), where dense unit indicate the positioning of spatial and channel attention; Deep interactive learning process (B) involves a baseline model trained on partially normal and a small amount of infertile mouse data, where histologists corrected the segmentation results of the baseline model and updated the training set after correction; Seminiferous tubule region segment (C), where internal cropping was performed in the network to improve mapping overlap and minimize boundary effects to further reduce boundary effects; Cell composition analysis of six testis cell types from the segmentation results (D).

TABLE 2 Quantitative results of testicular cell segmentation on Dataset 2 (D2).

Experiments	Model	PA	MPA	MIoU	FWIoU	CPA for spg	CPA for sc
Interactive learning	SCSD	0.956	0.801	0.689	0.930	–	–
	SCSD-Net+HIL	**0.967**	**0.827**	**0.713**	**0.932**	–	–
Ablation studies of SCSD-Net	RES-Net 50	0.951	0.725	0.663	0.924	0.762	0.569
	SE-Net	0.954	0.815	0.697	0.921	0.769	0.594
	SE-Net with dense block	0.957	0.818	0.706	0.925	0.772	0.617
Comparison with other models	U-Net	0.950	0.783	0.677	0.929	0.767	0.584
	Seg-Net	0.949	0.769	0.665	0.917	0.763	0.553
	U-Net++	0.948	0.781	0.672	0.911	0.761	0.569
	Attention U-Net	0.950	0.792	0.684	0.919	0.782	0.654
	SCSD-Net	**0.967**	**0.827**	**0.713**	**0.932**	**0.802**	**0.669**

Abbreviations: CPA, classification pixel accuracy; FWIoU, frequency-weighted intersection over union; MIoU, mean intersection over union.
The evaluation metrics shown in the table represent the mean of all test samples.
The bold values indicate values from the model this work develop, "SCSD-Net".
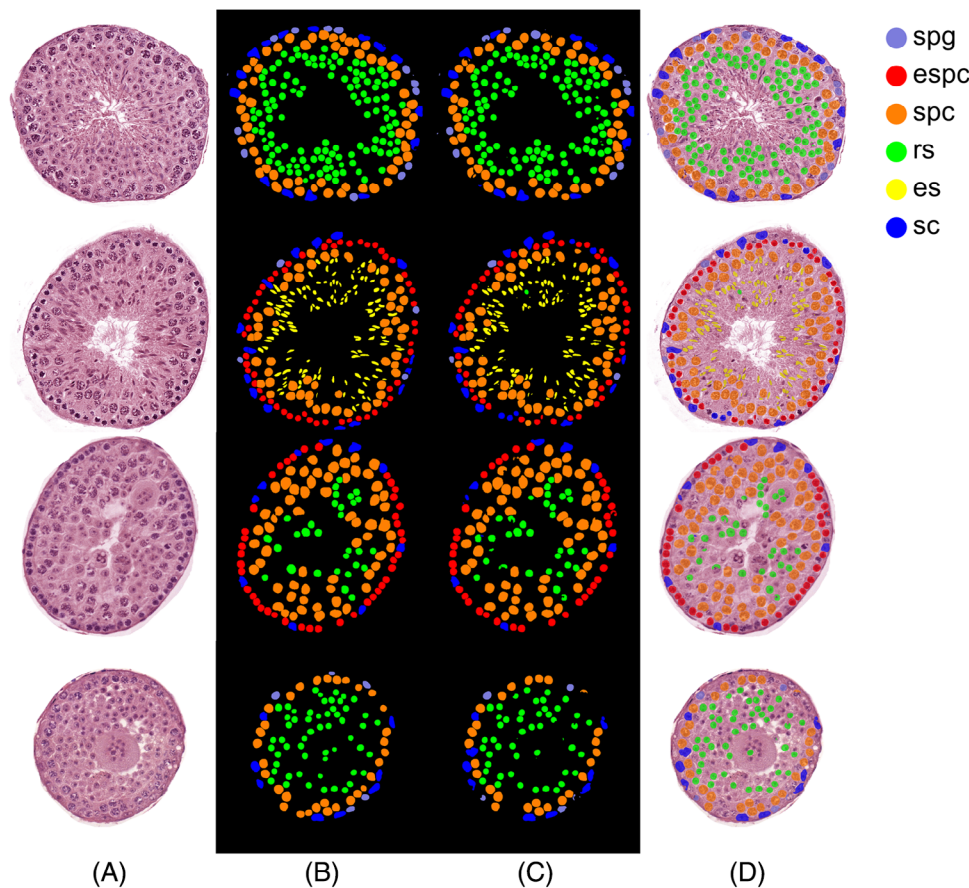
FIGURE 2   Results of qualitative analyses of representative tubules from wild-type (top two rows) and Boule knockout mutant (BKO). (A) Hematoxylin and eosin (H&E)-stained seminiferous tubule cross-section images, (B) showed annotation of the tubule section by marking six testicular cell types, (C) is result obtained by SCSD-Net+HIL (C) in D3. (D) A false-color map was obtained by superimposing the segmentation results of SCSD-Net-HIL on the original tubules (A). Blue color for SC (Sertoli cells), purple for Spg (spermatogonia), red for eSpc (early spermatocytes), orange for Spc (spermatocytes), green for RS (round spermatids), yellow for ES (elongating spermatids).

respectively. Our histologists, along with the qualitative segmentation results shown in Figure 2, are satisfied with its performance, deeming it sufficient for the automated segmentation of testicular cells in batches. Consequently, we employ SCSD-Net to segment testicular cells automatically in both wild-type and BKO mice for subsequent automated analysis.

2.2 | Evaluation of SCSD-Net-HIL model through cell composition analysis of a spermatogenesis-defective mutant, BKO

Previous studies have shown that the loss of BOULE protein in mammals can lead to spermatogenesis arrest at step 6 of the round spermatid stage (Figure 3A), resulting in male infertility.[32,36] While the specific arrest stage of spermatogenesis in BKO has been well-defined qualitatively, the quantitative cell composition of the BKO testis remained unknown. Therefore, we used the SCSD-Net-HIL model to perform a quantitative analysis of testicular cell composition in *Boule* gene knockout mice (BKO) and evaluate the effectiveness of our model.

When comparing nine sections of BKO testes (512 tubules) with wild-type mice (1245 tubules), we found a 45% reduction of the average number of testicular cells per round tubule section in BKO, consistent with the 48% reduction in the testis weight.[36] Overall, tubule distribution for the number of testicular cells per tubule was shifted toward the left in Figure 3B, with the highest number of tubules containing around 80 testicular cells in BKO mice, in comparison to 160 or 180 cells/ tubule being the highest number in wild-type mice.

To further evaluate the segmentation accuracy of SCSD-Net for the six types of testicular cells in BKO mice, we chose 30 VI to XI stage tubule sections from Dataset 3 (D3; Figure S1). We compared the results of cell composition analyses done by our histologist, our model (SCSD-Net+D3-Sub), and our model on all the VI to XI sections in D3 (SCSD-Net+D3). Figure 3C shows cell composition analysis results for each tubule cross-section image of D3-SUB, counted by the histologist (black bars) and SCSD-Net (gray bars) for the six testicular cell types.

We chose to annotate six testicular cell types, five spermatogenic cell types: spermatogonia, early spermatocytes (preleptotene, leptotene, and zygotene from Stage IX to XII), spermatocytes (pachytene and diplotene spermatocytes from all stages), round spermatids (round
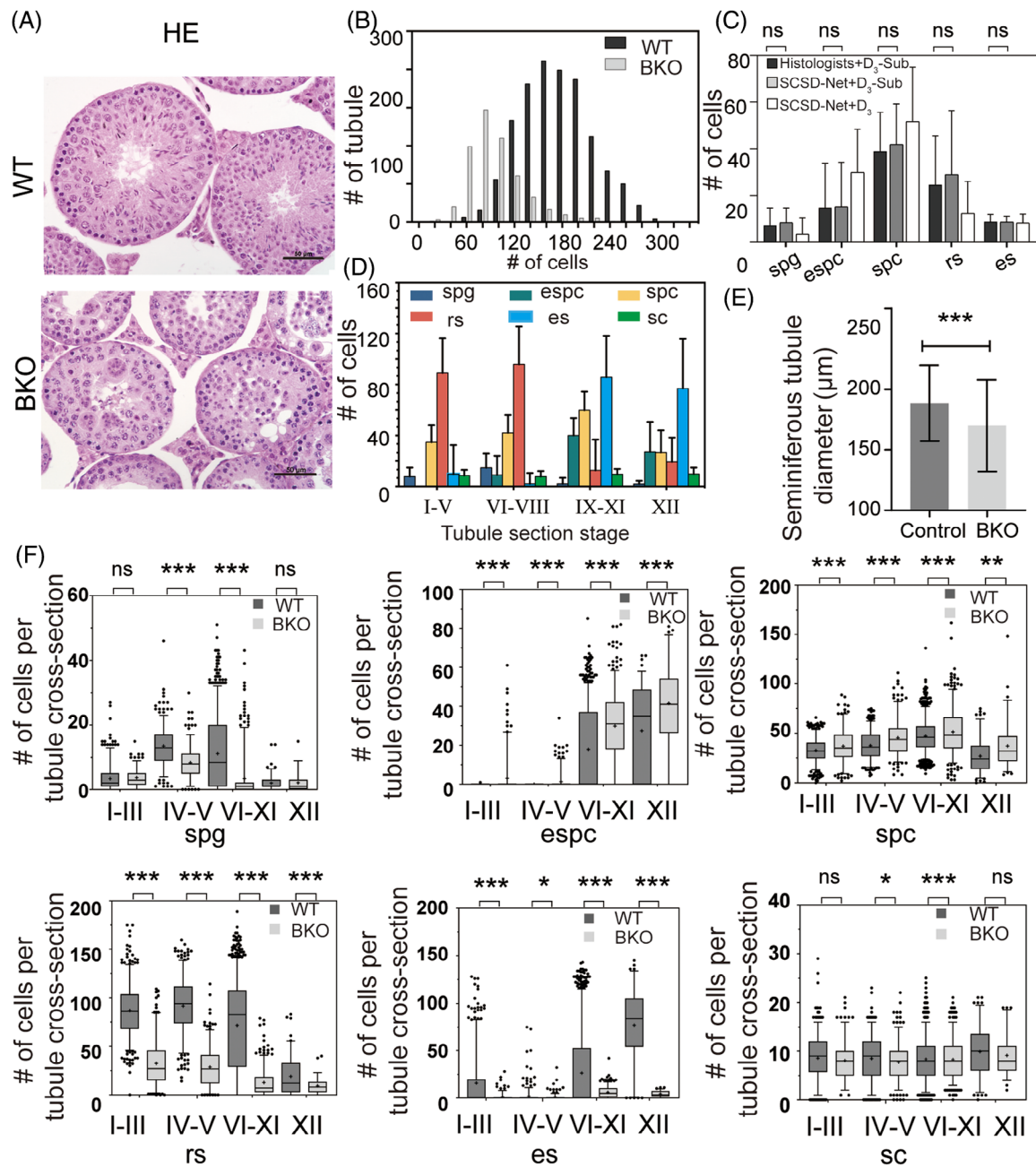
FIGURE 3 Quantitative analysis of cell composition in BKO and wild-type mice. (A) The hematoxylin and eosin (H&E) staining image of wild-type and BKO testis tubule cross-section, scale bar: 50 µm. (B) Distribution of tubules based on total cell # per tubule. BKO and wild-type mice are indicated as white and black bars, respectively. (C) The results of cell counting in D3-Sub by histologist and SCSD-Net, respectively, SCSD-Net+D3 is for all tubules in D3. The bar graphs and error bars showed the sample mean and standard deviation. Student's t-test for statistical results in Stages VI–XI. (D) Mean number of six testicular cells per tubule in wild-type mice in four stages groups. (E) The area of average seminiferous tubules of BKO and wild-type mice, error bars showed the SD. (F) Box plots of testicular cell counts in BKO and wild-type mice across four stage groups, whiskers: 5–95 percentile, "+" indicates mean value. p value evaluated by Student's t-test, *, p value <0.05; **, p value <0.01; ***, p value <0.001; ns, not statistically significant.

spermatids from Stage I to Stage VIII as well as secondary spermatocytes in St XII), elongating spermatids (elongating spermatids from Stage IX to XII), and Sertoli cell. Quantitative analysis of those five spermatogenic cell type and Sertoli cells provides cellular composition analysis of major developmental stages of spermatogenesis and represents an objective quantitative evaluation of spermatogenesis.

SCSD-Net+D3 (white bars) represents the analysis of all data (249 VI–XI tubules) in D3. The data in Figure 3C indicate no significant difference (ns) between SCSD-Net and histologists in cell composition analysis for BKO mice. The SCSD-Net+HIL model slightly identified a higher number of the five types of cells during the VI–XI stages than histologists (Figure 3C). Partially overlapping cells were delineated

and counted separately via a watershed function in SCSD-Net+HIL, possibly accounting for the increase in the number of cells in our model.

We next quantified the number of each cell type in four groups of neighboring epithelial stages using selected tubule sections and 30 VI–XI annotated by our histologists (Figure 3D and Table S3). Figure 3D illustrates the composition analysis of the six types of testicular cells by SCSD-Net for wild-type mice during stage groups (I–V, VI–VIII, IX–XI, and XII). The results demonstrate consistency in spermatogenesis among wild-type mice. The number of Sertol cells (sc), spermatogonia (spg), and spermatocytes (spc) are less fluctuated across the four groups (Figure 3D). Round spermatids (rs) are high in from Stage I to Stage VIII, but drop significantly in later stages, consistent with the development of round spermatids into elongated spermatids starting in st IX. The low number of rs in IX–XI and XII are due to sections in the transitional stage of VIII–IX or St XII–I, which will contain a good number of round spermatids.[37] The cell count of rs during Stages I–XII is slightly lower than the previously reported[38]; such difference could be attributed to less distinctive morphological features of rs due to fixation and staining as well as the difference in the mouse strains used. We further measured the diameter of the tubule section by taking the average of the long axis and short axis (Figure 3E). The average diameter of the *Boule* mutant seminiferous tubule was reduced by 10%, consistent with the significant reduction in testis weight.

Next, we would like to perform a quantitative comparison of cell compositional change stage by stage between BKO and wild type. Since BKO lacks all the elongating spermatids and round spermatids after step 6, yet the presence of round spermatids and elongating spermatids is one of the vital deterministic features of staging, we could only group several neighboring stages in BKO testis into four grouped stages: I–III, IV–V, VI–XI, and XII. We have utilized box plots in Figure 3F to display the mean, quartiles, and range of the number of the six cell types per cross-section in the testes of BKO and wild-type mice (nine cross-sections of D3). In most subgroups of the seminiferous tubules of both BKO and wild-type mice, the six testicular cell types showed significant differences between BKO and wt, but the most dramatic reduction in BKO is seen in round spermatids (rs) and elongating spermatids (es).

The quantity of rs in BKO mice is significantly lower than in normal control mice across all stages. In Stages I–III and Stages IV–V, the rs quantity is only 32.41 ± 24.09 and 28.61 ± 21.13 (mean $\pm$ SD), respectively, representing 62.7% and 68.8% lower than the corresponding control group quantities of 86.86 ± 26.47 and 91.78 ± 28.09 during the same stages. From Stage VI onward in BKO mice, spermatids commence development toward steps 7–12. The spermatid arrest occurring at spermatids (step 6) leads to apoptosis of spermatids in later steps. During Stages VI–XI, the quantity of rs in BKO mice is only 17.5% of that in the control mice. Such a dramatic reduction in spermatids is consistent with the global arrest phenotype at the round spermatid step 6 and lack of round spermatids after step 8.[36]

The number of elongating spermatids (es), corresponding to the elongating spermatids from Stage IX to XII, is a good indicator of whether spermatid elongation has occurred in the mutants. Indeed, in Stage XII, es dropped from 77.2 ± 38.98 in wild type to 4.4 ± 3.2 in

BKO, a 94% drop, consistent with the lack of elongating spermatids. In VI–XI stage group, there is a 77% drop in the number of es in BKO, despite a much bigger range of variation of es in VI–XI group. In this group, wild-type tubule sections from VI to VIII do not contain elongating spermatids while wild-type tubules from IX to XII will contain elongating spermatids, the average of es in wild-type group will hence be lower, leading to a smaller reduction of elongating spermatids when comparing BKO and wt than decrease percentage in BKO XII. The average number of sc in BKO showed slight but significant reduction in two out of four stage pools (Figure 3F). The average quantities of espc and spc showed a significant increase in the BKO relative to wt, with espc increase by 66.6% in St VI–XI, and 50.9% increase in St XII, raising the possibility of slow down of meiotic progress in BKO or disruption of seminiferous tubule organization due to global arrest of spermiogenesis or both (Figure 3F). The number of spg in BKO at St IV–V and VI–XI decrease by 37.7% and 68.6%, respectively. Such a quantitative difference in the average number of BKO spg, espc, and spc per section were not reported previously. Further characterization is needed to distinguish whether disrupted seminiferous tubule due to disrupted spermatogenesis or previously not appreciated spermatogenic defect contributes to the significant change in the average number of those cell types. Despite this, this cellular composition analysis clearly identified the absence of elongating spermatids and dramatic loss of round spermatids, consistent with the reported major defects of Boule knockout.

2.3 | Quantitative analysis of testicular defects from fertile mutant mice with reduced testis weight

2.3.1 | Generation of Sertoli-specific double knockout of *Pum1* and *Pum2* mice

To determine if *Pum1* and *Pum2* work synergistically in Sertoli cells to regulate testis weight, we crossed Sertoli cell-specific cre transgenic mice[39] into *Pum1^flox/flox^*; *Pum2^flox/flox^*. After several generations of crosses, we generated Amh-Cre *Pum1^flox/flox^*; *Pum2^flox/flox^* (AcDKO; Figure S4). We confirmed the loss of PUM1 protein in Sertoli cells but not in germ cells by immunohistochemistry. At postnatal day 1 (P1), loss of Sertoli cell *Pum1* is most evident as most *Pum1* protein in the P1 testis is from Sertoli cells. In contrast, germ cell *Pum1* is predominant in the adult testis, making the loss of Sertoli cell *Pum1* less pronounced (Figure 4A). We further confirm the reduction of PUM1 and PUM2 protein in the testis extract of AcDKO relative to those of their littermates (Figure 4B). Remarkably, the cell cycle negative regulator CDKN1B protein was significantly increased, supporting PUM1 and PUM2, both repressed the protein expression of this cell cycle inhibitor in Sertoli cells to regulate the proliferation of Sertoli cells.[33] We further confirmed that Sertoli cell proliferation was significantly reduced at postnatal days 4 and 10 (Figure 4H–J).

As expected, the testis weight of this AcDKO is significantly reduced while the body weight is unaffected (Figure S3). While the sperm count of AcDKO decreased compared with their littermates, neither
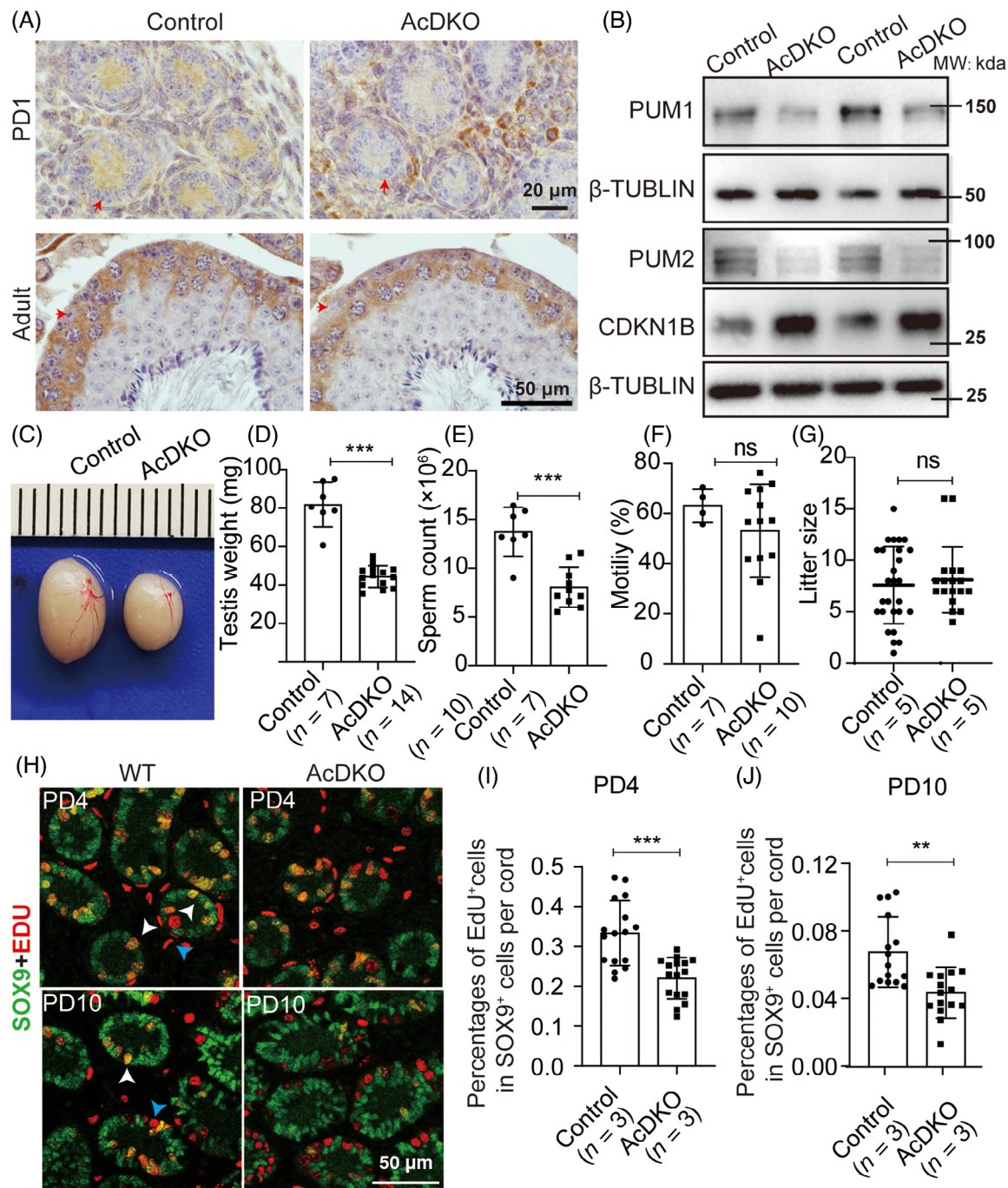
FIGURE 4 Generation and phenotypic characterization of Sertoli cell-specific knockout of Pum1 and Pum2 mice. (A) Immunostaining of PUM1 of the testis sections from wild-type and AcDKO mice at PD1(Postnatal Day 1) and adult age, red arrows indicated Sertoli cell PUM1; (B) Western blot showed that PUM1 and PUM2 protein was significantly reduced and CDKN1B protein was increased significantly in SC-DKO testes in comparison with those of wild-type control mice (P14); (C) Picture of AcDKO and control mice testes (12-week old); Testis weight ($p = 0.0001$, $N \geq 7$) (D), and sperm count ($p = 0.0001$, $N \geq 7$) (E) in AcDKO mice were significantly reduced. Motility ($p = 0.4719$, $N \geq 7$) (F), litter size ($p = 0.6176$, $N = 5$) (G) was not significantly different between control and AcDKO mice, Testes weight is the weight of one testis in one mouse. Motility is the percentage of motile spermatozoa in the cauda epididymis. (H) Immunofluorescence staining of EdU and SOX9 in cross-sections of testes from control and AcDKO males at PD4 and PD10; (I) Percentages of proliferative Sertoli cells in cross-sections of testes from control and AcDKO males at PD4, $n = (3, 3)$, $p = 0.0001$. (J) Percentages of proliferative Sertoli cells in cross-sections of testes from control and AcDKO males at PD10, $n = (3, 3)$, $p = 0.0011$; p value evaluated by Student's t-test, **, p value <0.01; ***, p value <0.001; ns, not statistically significant.

sperm motility nor fertility was significantly reduced from AcDKO (Figure 4E–G).

Given that AcDKO exhibited reduced Sertoli cell proliferation, we hypothesized that the reduced testis weight resulted from the reduced Sertoli cell number and spermatogenic cells. Hence, we turn to the SCSD-Net model to perform a quantitative analysis of testicular cells and uncover any spermatogenic defect inside the testis.

2.3.2 | Quantitative testicular analysis of AcDKO in comparison with AcP1KO and AcP2KO via SCSD-Net model

Since *AcPum1KO (AcP1KO)* and *AcPum2KO (AcP2KO)*, the individual knockout of *Pum* family members led to reduced Sertoli cell number and spermatogenic cells. Hence, we evaluate the reproductive defects of the AcDKO together with those of AcP1KO and AcP2KO to understand the effect of the loss of *Pum1* or *Pum2* or both in Sertoli cells.

We utilize the SCSD-Net model to perform quantitative cellular composition analysis as well as tubule diameter and area evaluation of testis sections from AcP1KO, AcP2KO, and the newly generated AcDKO (Figure 5B–D and Tables S4–S6). We chose those round seminiferous tubule sections (the ratio of the long axis over the short axis is between 0.8 and 1.2) to perform the analysis, as round tubules represent the cross-section of seminiferous tubules and minimize the number of distorted seminiferous tubules. AcDKO showed a consistent significant reduction in the average number of all cell types (spg, espc, spc, rs, es, and sc) per seminiferous tubule section with the biggest drop. The newly generated Sertoli cell-specific knockout of *Pum1* and *Pum2*, AcDKO, showed more reduction in the number of espc, spc, rs, es, sc, and total cells per section than either AcP1KO or AcP2KO (Figure 5B and Table S4), consistent with the synergistic action of *Pum1* and *Pum2* in Sertoli cells. Interestingly, while AcP1KO and AcP2KO did not show a decrease in the number of Sertoli cells per tubule section, there is a 11% decrease in the number of Sertoli cells per tubule in AcDKO, supporting a much more significant impact on Sertoli cell number per section in the absence of both Sertoli *Pum1* and *Pum2*. Considering the ease of analysis of our model on quantitation of cellular composition of the testis sections, we further explored to see if quantitation of staged round tubule sections will improve the detection of difference (Table S5). We chose round tubule sections from VI, VII, and VIII stages annotated by histologists and compared their quantitation from the testis sections of all three AcP1/P2/DKO with their littermate controls. While the overall trend stays the same using the staged tubule sections as the unstaged round tubules (Table S5 vs. Table S4), the variance of each cell type is significantly reduced when using staged round tubules. AcDKO has a 23% reduction in the number of rs when counting VI, VII, and VIII stage tubules combined and a 27% reduction in the number of rs when counting all round tubules. Both differences are statistically very significant, but the variance for rs in staged tubules is 23.3, and for all round tubules, it is 32.63 for AcDKO. This is consistent with much bigger variation in the number of rs and es from Stage

I to Stage XII than that among only Stage VI, VII, and VIII. Nonetheless, even without the separation of stages, our model could detect all the significant differences between AcP1/P2/DKO and their littermate controls. Hence, using our model with round seminiferous tubule sections with or without prior staging could represent a rapid method to perform spermatogenic analysis via testicular cell quantitation.

We further asked if we take in all tubule sections without the restriction on tubules being round (0.8–1.2; Table S6), we found that we still could detect all the differences detected by round tubule or staged tubule methods; the overall trend is very similar to what we saw with round tubules or staged tubules, but at a much higher variance. Intriguingly, all tubule quantitation revealed a significant difference in the number of Sertoli cells per tubule for AcP2KO at p value of 0.00155, while p value from the staged tubule method is 0.093 and 0.0589 for round tubules. This suggests that given enough tubule sections, the rapid nature of our SCSD-net model could be used to detect major reproductive defects affecting the cell number in the testis without applying strict selection criteria.

Diameter and area of the tubule sections for AcP1KO, AcP2KO, and AcDKO were also analyzed (Figure 5D and Table S7). The reduction in diameter and area is consistent with the decrease in the testis weight and total cell number reduction in each genotype. Hence, the diameter and area of tubules could be additional parameters our model could generate to determine the reproductive defects of mutant testes.

We next used wild-type testis sections to evaluate the impact of the number of tubules used on the average number and variance of each cell type per tubule and to determine the minimum number of tubules needed to achieve a stable representation of testicular cellular types with all tubules, round tubules, and staged tubules. Figure S5 showed data for all three methods with increasing tubules used for the same wild-type tubule data. Approximately in all tubule methods, when we reached 450 tubules, the average number of each cell type did not change with further increasing of tubules; while for round tubules, you need 300 tubule sections, and for staged tubules, we need 250 tubules to reach the stable estimate of all cell types (Figure S5). If we plot the mean and variance for all four cell types at the minimum number of tubules required for optimal stable counting for each method (450 tubules for all tubules, 300 tubules for round tubules, 250 tubules for Stage VI–VIII tubules; Figure S6), we found that the means for spc, sgsc, and sc do not differ much among the three counting methods. Still, the mean rspd number is much higher from the staged tubule method than all tubule or round tubule methods, consistent with the biology of seminiferous tubules staging where round spermatids are absent in St IX, X, XI, and low at St XII, reducing the mean of rspd when counting all tubules. The standard deviation is the least in staged tubule method for all the cell types.

2.4 | Detection of novel reproductive defects from sterile males lacking both *Boule* and *Dazl* at meiosis

While AcP1/P2/DKO affects the total cell number of each of the cell types in the testis, they do not cause any disruption of spermatogene-
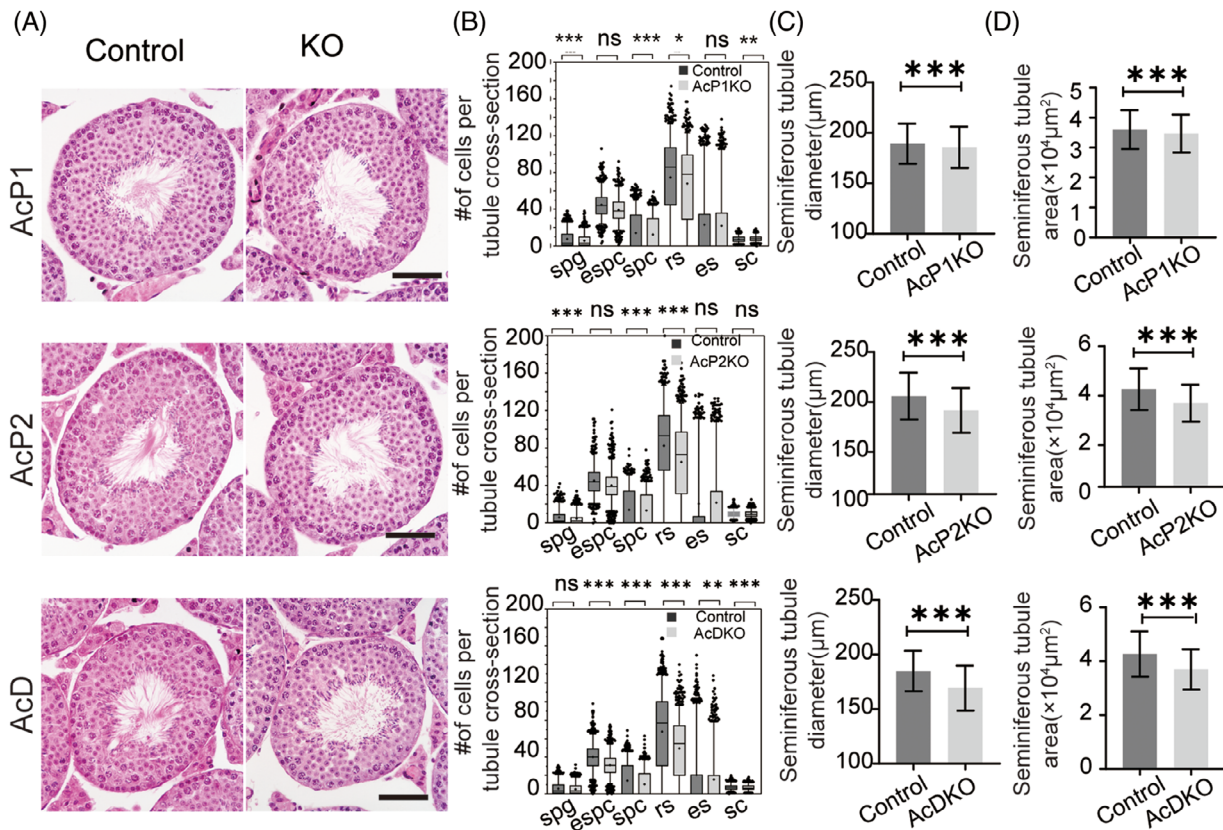
FIGURE 5 Quantitative analysis of cell composition of Sertoli cell-specific knockout of *Pum1*, *Pum2*, and both *Pum1/2*. (A) The hematoxylin and eosin (H&E) staining image of AcP1KO, AcP2KO, and AcDKO testis tubule cross-section and control in VII, scale bar: 50 μm. (B) The cell number of spg, espc, spc, rs, es, and sc were reduced significantly in AcP1KO ($N = 3$), AcP2KO ($N = 3$), and AcDKO($N = 3$), the number of sc was reduced significantly in AcDKO, no significant changes in AcP1KO and AcP2KO when compared with control. (C) The diameter of average seminiferous tubules was reduced significantly in AcP1KO ($N = 3$), AcP2KO ($N = 3$), and AcDKO ($N = 3$) when compared with control. (D) The area of average seminiferous tubules was reduced significantly in AcP1KO ($N = 3$), AcP2KO ($N = 3$), and AcDKO ($N = 3$) when compared with control.

sis, and none of the cell types are missing in the testis. A great number of mutations of reproductive genes, when knocked out, caused severe spermatogenic defects, leading to a significant reduction of one or more cell types and even a global halt of spermatogenesis. Hence, we tested our quantitative model on its ability to detect spermatogenic defects in sterile mice with severe reproductive defects. Previously, we have found that the knockout of members of the mouse *DAZ* family proteins in postnatal testes, *Dazl* KO and *Boule* KO, respectively, causes male sterility and global arrest of spermatogenesis.[29,32,36] Removal of *Dazl* at the spermatocyte stage with *Hspa2-cre*, full knockout of *Boule*, each led to complete male sterility and an arrest at the round spermatid stage.[29,32,36] Since both DAZL and BOULE are expressed in spermatocyte stage, and fly *boule* knockout produces a meiotic arrest phenotype,[40] it was proposed that DAZL and BOULE in mammals might work together during meiosis, lack of meiotic arrest phenotype in either *Boule* knockout or *Dazl* knockout may result from the redundant function of *Dazl* and *Boule*.[36] Hence, we decided to address this functional redundancy question through the generation of an animal lacking both *Dazl* and *Boule* in the spermatocyte stage.

We utilized a spermatocyte-specific cre transgenic mice, *Hspa2-cre*, *Dazl*[flox/flox] mice and fertile *Boule*^{−/−} female mice to generate a mutant lacking both *Dazl* and *Boule* in spermatocyte (*Hspa2-cre*, *Dazl*[flox/−] *Boule*^{−/−}, called HDBKO, for mating scheme, see Figure S7).[29] The genotype of the generated mice was confirmed by polymerase chain reaction (PCR) using tail genomic DNA (Figure S7). As expected, the Cre-mediated excision of the floxed alleles occurred only in the presence of the Cre transgene, resulting in the knockout of *Dazl* in spermatocytes of *Boule* knockout mice.

Next, we evaluated the fertility of HDBKO males by mating them with wild-type females. Despite regular mating with wild-type females for over 8 months, HDBKO males failed to produce any offspring, indicating complete male sterility. To assess the spermatogenic defects leading to sterility in these mice, we performed histological analysis of testis sections. H&E staining of testis sections revealed a severe disruption of spermatogenesis in HDBKO mice (Figure 6A). Unlike the control mice with normal spermatogenesis, HDBKO testes exhibited a lack of mature spermatozoa in the seminiferous tubules, indicating a global arrest of spermatogenesis.

We then employed the SCSD-Net model to perform quantitative analysis of testicular cell composition in HDBKO mice as well as spermatocyte-specific knockout of Dazl for comparison (Figure 6B) to gain insights into the specific cellular defects underlying male sterility.
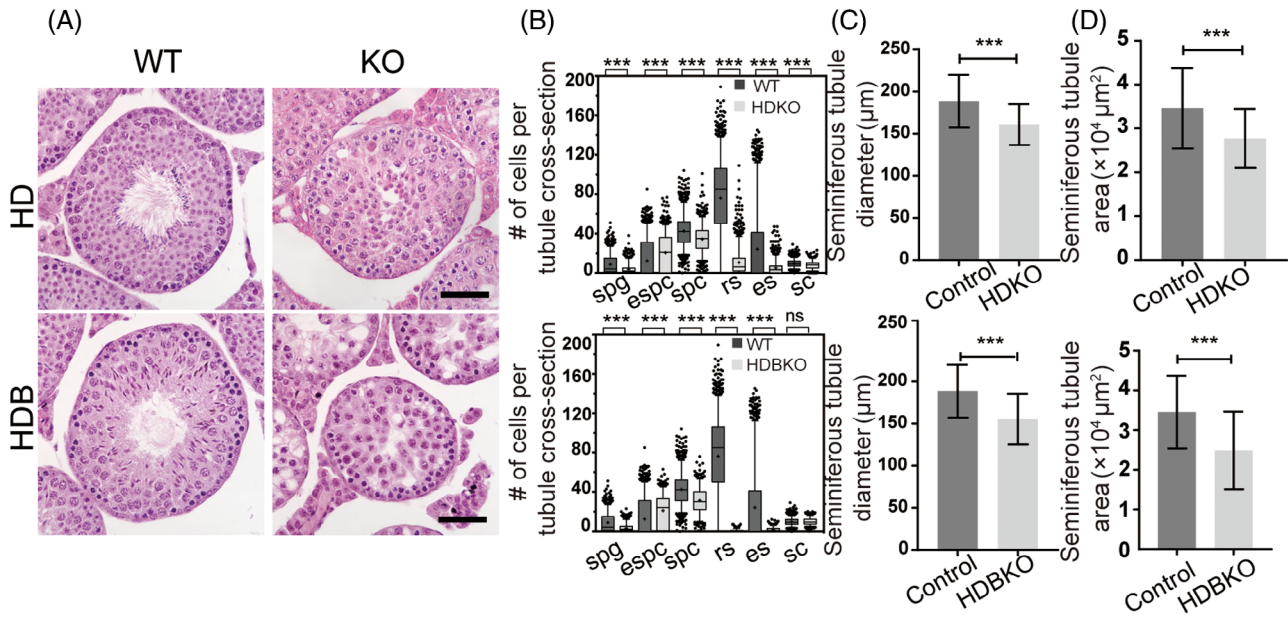
FIGURE 6 Quantitative analysis of cell composition in HDKO($N = 3$), HDBKO($N = 2$), and wild-type mice($N = 4$). (A) The hematoxylin and eosin (H&E) staining image of HDKO, HDBKO, and control testis tubule cross-section, scale bar: 50 μm. (B) The cell number of spg, espc, spc, rs, es, and sc were reduced significantly in HDKO and HDBKO. (C) The diameter of average seminiferous tubules was reduced significantly in HDKO and HDBKO, when compared with control. (D) The area of average seminiferous tubules was reduced significantly in HDKO and HDBKO when compared with control.

Our round tubule quantitative results showed a significant reduction in the numbers of early spermatocytes (espc), spermatocytes (spc), round spermatids (rs), and elongating spermatids (es) as well as in the diameter/area of seminiferous tubules in HDBKO mice compared with control mice (Figure 6B,C, Tables S8 and S9). The huge reduction in round spermatids and elongating spermatids to almost the baseline indicated an absence of spermatids and, hence, a meiotic arrest phenotype in these mice, consistent with the observed sterility. Overall, our quantitative analysis using the SCSD-Net model successfully identified and characterized the severe spermatogenic defects leading to male sterility in HDBKO mice.

2.5 | Proposed workflow for fast detection of reproductive defects

It is well established that Sertoli cells are the key determinant of the amount of sperm production, and the number of spermatogenic cells per Sertoli cell is a species-specific characteristic.[41–43] In our quest to efficiently detect reproductive defects, we transitioned from per tubule quantitation to a more reflective per Sertoli cell quantitation, which allows for a finer assessment of spermatogenic disruptions and serves as a spermatogenic index for the extent of spermatogenic defect among different mutants. By comparing the number of each cell type per Sertoli cell across six different knockout mice and their respective controls (Figure 7), we discerned distinct reproductive phenotypes. Specifically, HDBKO exhibited a notable absence of round spermatids, indicating lack of postmeiotic spermatids. BKO and

HDKO, on the other hand, have round spermatids but at a significantly reduced level; such a significant reduction of spermatid development is indicative of extensive loss of spermatids and completion of meiosis.

Notably, for the fertile mutants with no spermatogenic arrest, AcP1KO, AcP2KO, or AcDKO showed only marginal reductions in the spc/sc or sgsc/sc ratio, suggesting a quantitative decrease in cell numbers without apparent abnormalities in spermatogenesis. However, despite the significant reduction in rspd/sc, spc/sc, and sgsc/sc in the AcDKO, the similar reduction among all the three cell types suggested reduced functionality of Sertoli cells without any significant defect in spermatogenesis or any cell type. Such a mild or little effect on spermatogenesis is even more obvious when we compare the spermatogenic index from staged tubules for AcP1KO, AcP2KO, and AcDKO (Figure S8). The spermatogenic index in AcDKO is not different at all from controls in rspd/sc, spc/sc, and sgsc/sc, supporting undisrupted spermatogenesis in AcDKO other than smaller tubules and small total cell number per tubule (Figure S8) while AcP1KO and AcP2KO are slightly reduced in spc and sgsc. Since AcP1Ko, AcP2KO, AcDKO are all fertile with no obvious spermatogenic disruption, we could use the percentage of change in spermatogenic index of all the fertile mutants (less than 20%) as a baseline for normal spermatogenesis (Figure 7). We propose 50% or more reduction in spermatogenic index for any cell type as severe reduction of the cell type, 90% or more reduction as the absence of the particular cell type. Hence, a disproportional decrease or increase in spermatogenic index for any cell type per sc could be a strong indicator of spermatogenesis defects affecting one or more stages of spermatogenesis, while a proportional
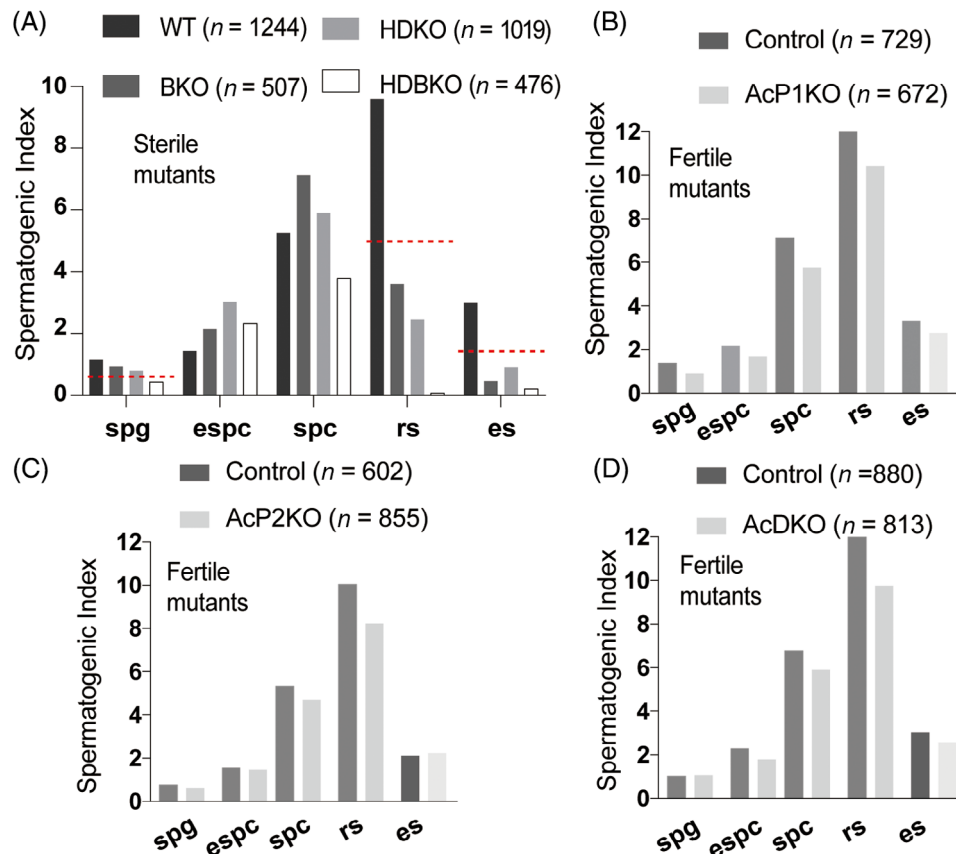
FIGURE 7 Quantification of spermatogenic defects in the mutants using spermatogenic index. (A) Quantification of germ cells per Sertoli cell in tubule cross-section of the testes from WT and BKO, HDKO, HDBKO male mice. The bar graph showed the ratio of average cell number of each cell type per Sertoli cell per section for wild type and three sterile mutants with disrupted spermatogenesis. As a comparison, spermatogenic index for all the cell types in three fertile mutants with only reduced testis size but no spermatogenic arrest were shown. When spermatogenic index for cell type of a genotype falls below the dotted red line, marking the middle point of wild-type value, indicating a spermatogenic defect in the number of the cell type. Dotted red lines indicating 50% reduction of spermatogenic index. (B) From WT and AcP1KO male mice. (C) From WT and AcP2KO male mice. (D) From WT and AcDKO male mice. Fifty percent reduction in spermatogenic index of a mutant could be clearly distinguishing sterile mutants with disrupted spermatogenesis from all three fertile mutants.

decrease per sc by 20% or less is indicative of minimal or no effect on normal spermatogenesis. This shift in focus toward Sertoli cell-based quantitation using this spermatogenic index could help swiftly identify spermatogenic defects without even going through staging. The testicular cellular composition analysis including spermatogenic index analysis represents an efficient protocol for identifying spermatogenic defects from H&E-stained testis sections from both mutant and littermate control mice through our SCSD-net model (graphic abstract). By choosing either staged tubules, unstaged round tubules or unstaged all tubules from 8 to 10 H&E-stained testis sections, we could achieve a quick assessment of spermatogenic defects in the mutants via cell composition analysis of the testicular tubules in as few as 3 h. The number of four testicular cell type per tubule and diameter/area of tubule sections could provide quantitative changes of spermatogenesis in the mutant while the ratio of each cell type over Sertoli cell number per tubule, as a spermatogenic index, will reveal any qualitative defects on cell types if any disproportional change occurs in any of the cell type.

3 | DISCUSSIONS

The quantitative analysis of seminiferous tubule sections using deep learning models presents a promising advancement in histopathological assessments, offering both rapidity and potentially heightened accuracy compared with traditional methods conducted by experienced histologists.[11–17,19,20] By integrating an interactive learning strategy into our SCSD-net model for quantitative cellular analysis of mouse testis and incorporating mouse mutant testis in our training dataset, we enhanced the pixel accuracy of testicular cell types, reduced histologist annotation time, and established a novel model for quantitative and qualitative analysis of reproductive defects from H&E testis sections.

We validated the effectiveness of our SCSD-net model by analyzing six mouse reproductive mutants with various spermatogenic defects, proposing a workflow for the quantitative and qualitative assessment of histopathological defects using 8–10 H&E testis sections from both mutants and controls within a few hours. While manual epithelial

cycle staging is essential for histological analysis of mammalian spermatogenesis and pathological examination of male infertility, it is time consuming and requires extensive training. Our and others' efforts in developing deep learning models aim to establish automatic or semi-automatic staging systems for wild-type mice and rats.[12,14,15,17]

Although some models have focused on the most used H&E-stained testis sections for staging and cell type segmentation, others have utilized fluorescent chromatin stain—DAPI-stained testis sections for combined staging and cell type analysis.[15,17] However, accurate staging of all 12 stages may be difficult or even impossible to achieve for reproductive mutants with severely disrupted spermiogenesis, even with the aid of PAS-staining, testicular cellular composition analysis focusing on several major spermatogenic cell types could provide highly needed quantitative evaluation of spermatogenesis, independent of staging. Such statistical extraction on mutant H&E sections has often been lacking, leaving the effectiveness of these models in detecting reproductive defects unknown. In our study, we systematically evaluated the efficacy of our SCSD model on six mouse mutations, demonstrating its effectiveness in both quantitative and qualitative analysis of mutant testes through commonly used H&E staining protocol.

We identified novel spermatogenic defects in two previously uncharacterized double mouse mutants on the mouse *DAZ* family and *PUM* family, supporting the requirement of synergistic interaction between Sertoli *Pum1* and *Pum2* for normal sperm production and the redundant function of DAZL and BOULE for meiosis in mice. The precise removal of *Pum1* and *Pum2* in Sertoli cells reduced the testis size further than the removal of either *Pum1* or *Pum2* alone yet without any detectable effect on spermatogenesis, providing convincing evidence for Pum1/2 as dosage-dependent Sertoli factors regulating testis size.[33] Our deep learning model showed clearly that PUM-mediated testis size regulation is achieved through a wholesome reduction of the number of Sertoli cells and different types of spermatogenic cells per tubule as well as the reduction of diameter of tubule and tubule area in the mutants yet maintains the same ratio of Sertoli cells and spermatogenic cells as in wild type. Mechanistically, PUM1/2 regulates Sertoli cell proliferation through their downstream cell cycle targets, most prominently Cdkn1B expression at post-transcriptional level.[33] Our work provided a clear case how Sertoli cell factors regulate the gonadal size at molecular, cellular, organ, and physiological levels to control sperm production, further study of PUM-mediated translation in gonadal size regulation among different species may help to understand the evolutionary basis of gonadal size variation and their relationship with sexual selection. Such RNA-binding proteins mediated translational control of organ size in a single cell type may also be of general significance in our study of organ size regulation in general.

The novel meiotic arrest defect in the absence of both *Dazl* and *Boule* in the spermatocytes uncovered the redundant functional requirement of *Dazl* and *Boule*, which have been long suspected,[36] and support the notion that the ancestral function of the *DAZ* family is at meiosis, and both *Dazl* and *Boule* participate in mouse meiosis regulation. Our testicular cellular composition analysis not only uncovered the global

arrest of spermatogenesis in the double mutants but also quantitative changes in other spermatogenic cell types, further study is needed to determine whether those changes in other spermatogenic cell types resulted from secondary effect of cellular organization change inside the testis or the direct effect of the mutations.

In terms of reliable representation through quantitative analysis, we found that by counting a minimum number of tubule sections, we could achieve stable data representation of the average cell numbers of each of the four testicular cell types. Varied tubule selection criteria, including all tubules, only round tubules, or tubules of specific stages, impacted variance in means of each cell type while exhibiting a similar power in detecting quantitative differences in mutant testes. Remarkably, counting all tubules, including longer ones, proved as effective as using selectively round or staged tubules to identify the significant spermatogenic defects, allowing users without prior knowledge of testicular histology to conduct quick analyses and identify defects promptly.

Even for the previously characterized mouse mutants, our model not only revealed quantitative differences of each of the six testicular cell types in the mutants, consistent with their known spermatogenic defects but also identified statistically significant differences among most cell types. While we utilized unpaired Student's *t*-test for our testicular cellular composition comparison between mutant and control, we have used other statistical methods, including Welch two sample *t*-test and Wilcox test group, to validate the *t*-test results. The large sample size of tubules used in the analysis significantly increase the sensitivity for those groups with only a small difference in mean but a large standard deviation. Some of the difference may represent previously not appreciated biological defects between the genotypes. For BKO, besides the significant reduction of round spermatids per tubule, we also detected a significant reduction of spg, although small, in Stage IV–V and Stage VI–XI, as well as an increase in espc and spc. This suggest that while spermiogenesis is blocked in BKO, sperm development before meiosis may have also been impacted to some extent. Alternatively, the seminiferous tubule organization has been affected due to the disruption of spermiogenesis, contributing to such a change in the average number of other cell types per section.

Our future direction involves extending the automation process to combine staging all 12 stages of tubule sections with the cell type analysis, providing a comprehensive and rapid quantification of each stage and analysis of between 10 and 20 different cell types. We aim to establish an interactive web version for users to upload their H&E-stained testicular sections, benefitting individuals in areas with limited resources. Additionally, we plan to refine our model by training on other mutant mice, including HDKO and HDBKO, to address current limitations and enhance accuracy in detecting abnormalities in testicular development.

In conclusion, our refined approach, employing per Sertoli cell quantitation and selective tubule analysis, enables rapid and accurate detection of reproductive defects within a few hours. Our methodology offers a well-represented quantitative and qualitative histological evaluation of mutant testes within a short period, aiding histology labs in quick histopathological diagnoses of mouse testes from mice with

mutated genes or from environmental toxicology. This study marks a significant advancement in testicular pathology tools, introducing a rapid and efficient protocol for quantitative analysis of seminiferous tubule sections using deep learning models to enhance the speed and accuracy of spermatogenic defect detection.

4 | MATERIALS AND METHODS

4.1 | Materials

4.1.1 | Antibody and reagent

Antibodies used in this manuscript are as follows: Abcam: PUM1 (ab92545) 1:100 immunohistochemistry (IHC), 1:500 western blot (WB); Millipore: SOX9 (AB5535) 1:2000 IF; Hartman's Fixative Sigma-Aldrich Cat#H0290; EdU (C00053); Cell light EdU Apollo 567 (C10371-1).

4.1.2 | Animals

Animals were housed under controlled environmental conditions in the animal facility of Nanjing Medical University, Nanjing, China, with free access to water and food. Illumination was provided between 8 AM and 8 PM daily. All animal experiments were approved by the Animal Care and Use Committee (ACUC) of Nanjing Medical University.

Amh-cre mice and *Hspa2-cre* were obtained from Jackson Lab and Model Animal Research Center of Nanjing University. Sertoli cell-specific *Pum1* and *Pum2* double knockout (AcDKO) mice were created by crossing *Amh-cre* transgene mice with *Pum1^{F/F}* and *Pum2^{F/F}* mice, respectively.

4.2 | Methods

4.2.1 | Experimental settings

Seminiferous tubule region segmentation
Segmentation of seminiferous tubules is crucial for ensuring the integrity of testicular cells within each tubule. During the training phase, chromatic standardization is employed to address data variations from different batches. We downsampled each WSI and obtained image patches at 20× magnification (Figure 1C). To avoid border effects, we initially filled the images with a white background and subsequently fed the image patches and masks corresponding to them into the network for training. Finally, the edited segments are integrated into the canvas and resized to match the original image dimensions. In preparation for training, we annotate the boundaries and interiors of the tubules separately, utilizing the boundaries as a training background. Subsequently, we employ post-processing techniques to rectify shortcomings in tubule segmentation and inter-tubule adhesion.

SCSD-Net architecture
To address the challenges of precisely delineating nuclear boundaries in the testes of infertile mice and categorizing nuclei into different classes, we propose an encoder–decoder-style deep neural network named SCSD-Net. This network integrates SE modules and attention-dense units (Figure 1A) to enhance the segmentation and classification performance of the network. The SCSD-Net is designed to regress nuclear regions simultaneously and perform nuclear-type segmentation. The U-shaped architecture of this network enables accurate semantic segmentation of images.

The feature learning network is based on ResNet50,[44] and consists of multiple SE-Res[45] residual convolutional blocks for the segmentation task. The network undergoes four down-sampling operations for each seminiferous tubule image to extract high-dimensional features, followed by batch normalization (BN) and Leaky ReLU activation functions. Pixel-level predictions are obtained through the decoder, with two task branches for nuclear region segmentation and cell classification. Dense units with attention activation are integrated into the decoder to better capture relationships between input features.[46] Channel attention enhances the responses of important channels while suppressing those of irrelevant channels, and spatial attention enhances responses at crucial locations while suppressing responses at irrelevant locations. Both attention mechanisms help the model better capture local and global dependencies in the input data, thereby improving model performance,[47] recognizing that attention mechanisms not only enhance the classification performance of convolutional neural networks (CNNs) but also bolster their robustness to noisy inputs.[48] Thus, we incorporate attention into the decoder branch to generate unique attention maps for accurately detecting adhered and overlapping nuclei.

Deep interactive learning
To strike a balance between accuracy in recognition and generalization of the model, we employed a HIL learning strategy (Figure 1B). Specifically, we started by establishing a baseline model using a small amount of mouse data to segment six testicular cell types. Upon applying this model directly to knockout mice, we observed certain errors such as insufficient segmentation of sc, misidentification of rs, and misclassification of some sg and espc. In such cases, a histologist visually assessed the segmentation results. High-quality segmentation results were incorporated directly into the training set after fine-tuning, while segmentation errors, often involving challenging and rare features, required the histologist to re-annotate or correct the existing predictions before being added to the training set. This human–machine interactive process iterated multiple times until the model achieved the desired performance. In the training of the new model, we employed a reduced learning rate and extended the training epochs to enhance stability.

Cell composition analysis
Based on the segmentation of the testis cells obtained from the model, we will conduct an analysis to examine their cell composition. Objective metrics such as mean, variance, and cell area proportion to investi-

gate the quantities of the four types of testicular cells across different stages:

1. Comparative analysis of the cellular composition of the six types of testicular cells in different seminiferous tubules at four stage groups in BKO mice.
2. Comparative analysis of the composition of the six types of testicular cells in cross-sections of seminiferous tubules in BKO/HDKO/HDBKO and AcP1/P2/DoubleKO mice.

Data preparation

All WSIs of mouse testicular cross-sections used in this study are obtained from the State Key Laboratory of Reproductive Medicine in Nanjing Medical University. Testes were fixed with Hartman's Fixative (Sigma, H0290) overnight then dehydrated prior to paraffin embedding. Tissue was rinsed in 70% ethanol (EtOH) then dehydrated for 30 min in 70% EtOH, 30 min in 80% EtOH, 30 min in 95% EtOH, 2× 30 min in 100% EtOH, 30 min in xylene then briefly dipped in melted paraffin and incubated in paraffin 2 h at 60° then embedded in paraffin blocks. Five micrometer sections were cut and stained with H&E after being dewaxed and rehydrated. Images were captured using a 3DHIS-TECH Pannoramic SCAN II at 40× magnification (0.23 µm/pixel) and processed with ImageScope software. The size of each digitized WSI was approximately $15,000 \times 20,000$ pixels.

The opinions of histologists with extensive experience in identifying different cell types were used as a reference point to minimize differences between annotators during the annotation process. The detailed descriptions of the datasets used in this study are as follows:

D1 and D2 were manually annotated by our histology expert, who has 5 years of experience in mouse testicular histology. In the annotation process for D2, ST images were categorized into five classes: four testicular cell types (sgsc in red, spc in orange, rspd in green, and sc in blue), and a black background. D3 was manually staged by histologists Min for BKO mice. The staging annotation for the control group's wild-type mice was collaboratively completed by another mouse histology expert, Dr. Dirk de Rooij, who has decades of experience in mouse testicular histology, and our histologist. Non-vertical cuts of testicular cross-sections can result in atypical seminiferous tubules. To eliminate the impact of atypical tubules, we manually removed these tubules from D3, D4, and D5. The first and second rows of Table S2, respectively, exhibit the number of tubule images before and after removing atypical tubules.

Implementation details

The end-to-end neural network model, SCSD-Net, proposed in our study, was specifically designed for the segmentation and analysis of four testicular cell types. We implemented SCSD-Net using the open-source machine learning framework PyTorch (version 1.13.1) and conducted training and testing on a system equipped with an 11th gen Intel® Core™ i7-11700 CPU (2.50 GHz) and an NVIDIA GeForce RTX 4090 GPU (with a 24 GB memory capacity). The learning rate was set to 0.0002, the training batch size was set to 100, and we employed Ranger as the optimizer. Due to hardware limitations, we constrained the batch size to three images.

4.2.2 | Experimental design and comparison strategies

SCSD-Net with deep interactive learning

Interactive learning can significantly alleviate the annotation workload for histologist. This experiment aims to demonstrate how interactive segmentation effectively enhances the performance of SCSD-Net in the segmentation of the testicular cell types. We compared the segmentation performance of the network with deep interactive learning (SCSD-Net+HIL) and without deep interactive learning (SCSD-Net). In the experiment without deep interactive learning, SCSD-Net used our pre-existing labeled data from typically developed wild-type mice alongside partially unlabeled data from genetically defective mice. The quantities of the six testicular cell types before and after interactive learning are detailed in Table S1.

Ablation experimental study of SCSD-Net

This experiment evaluated the effectiveness of SE-RES, dense block, and Channel and Spatial attention block (CS block) in segmentation. SCSD-Net was compared with Res-Net50, SE-Net, and SE-Net with attention-dense block and three different models. Additionally, the impact of different numbers of dense units (0, 1, 2, 3) on model training time and performance was compared, and two dense blocks were eventually chosen. The evaluation of all models was based on data undergoing interactive learning.

Comparison with other models

These experiments aim to verify the enhanced segmentation performance of SCSD-Net in comparison to four state-of-the-art models: Seg-Net,[49] U-Net,[50] U-Net++,[51] and Attention U-Net.[52] Additionally, a distinct evaluation was conducted for the segmentation results of sgsc and sc. By comparing it with the mentioned models, this demonstrates that SCSD-Net can effectively segment these two challenging cell types. The data used for the models had undergone the interactive learning process.

Cell composition analysis of the seminiferous tubules of BKO mice at Stages I–XII

This research aims to assess the SCSD-Net+HIL model against professional histologists in quantitatively analyzing testicular cells in infertile mouse testes. Due to the arrested development of spermatogenesis at the round spermatids in the testes of the knockout mice, detailed classification based on the morphology and arrangement of sgsc and spc is challenging for certain stages. Manual analysis of testicular cells numbers in all nine testicular cross-sections is difficult for histologists. We selected a subset of images from the VI–XI stages of seminiferous tubules as D3 (Sub-D3) to address this. The SCSD-Net+HIL model was employed to automatically segment the four types of testicular cells in D3 and Sub-D3 seminiferous tubule

images. Subsequently, quantitative analysis was conducted on the cells. To explore the developmental changes in the number of testicular cell types in the entire testicular cross-section seminiferous tubules of wild-type and BKO mice at different stages, we employed the SCSD-Net+HIL model to automatically segment the four testicular cell types in the seminiferous tubules of both mouse genotypes over Stages I–XII. Subsequently, quantitative analyses of testicular cells in the nine cross-sections of D3 were performed for both mouse genotypes, exploring the effects of gene knockout on mouse cell composition.

4.2.3 | Histology, immunohistochemistry, and immunofluorescence

Tissues were fixed overnight in Hartman's fixative (Sigma). Fixed testis was embedded in paraffin and cut into 5-μm-thick serial sections; sections were processed for H&E staining and IHC, IF according to standard protocol.[14] The number of testis sections and tubules used and the number of animals for each genotype is listed in Table S11. Immunostaining for PUM1 was performed, following citrate buffer antigen retrieval, by incubation with anti-PUM1(1/100, Abcam) and anti-SOX9 (1/1000, Millipore) primary antibodies and detected using Biotin–Streptavidin HRP Detection Systems (ZSGBBIO). A minimum of three randomly chosen discontinuous sections were used to determine positive cells in tubules.

4.2.4 | 5-Ethynyl-20-deoxyuridine assay

5-Ethynyl-20-deoxyuridine (EdU; RIBOBIO, C00053) treated mice at a dosage of 50 mg/kg body weight through intraperitoneal injections. Three hours after EdU injections, testes were collected. Before EdU detection, immunofluorescent staining of SOX9 was carried out. Then, EdU was detected according to the manufacturer's instructions for Cell LightTM EdU Apollo 567 in vivo Kit (RIBOBIO, C10371-1).

4.2.5 | Fertility test and sperm count and motility analysis

Adult control mice AcDKO males (10–12 weeks old) were mated with 6–8 weeks old wild-type ICR female mice. One male was mated with two ICR females for 6 months. Five WT control and five AcDKO animals were used in the fertility test. Average litter size and litter size numbers were recorded to assess fertility. For sperm motility, one cauda epididymide was dissected and incubated at 0.2 mL in HTF (Aibei, M1130) at 37°C for 5 min. Sperm motility was measured with a computer-aided sperm analysis (CASA) machine (Hamilton Thorne). The remaining sperm sample was used for sperm count by hemocytometer.

4.2.6 | Quantification and statistical analysis

All data in bar and line graphs are expressed as means $\pm$ SD (standard deviation of the mean). A minimum of three animals per genotype are used for each experiment, the specific number of animals are listed in Table S10 for cell composition analysis and figure/legend for AcDKO characterization. More than 200 seminiferous tubules per testis were used for Sertoli cell counting of AcDKO characterization. The average number of tubules used to analyze germ cell number per cord was more than 600 per mouse. The number of Sertoli cells used to quantify percentage of EdU+ cells in SOX9+ cells was more than 2000 for each mouse, recorded by the percentage of EdU+ SOX9+ cells to the SOX9+ cells in the 40× objective image. The diameter and area of the seminiferous tubule section were determined based on the circumscribed rectangle of the tubule section. The tubule cross-section diameter was determined based on the average of the horizontal axis and the longitudinal axis of the rectangle immediately outside the seminiferous tubule section. The area is the product of the rectangle's horizontal axis and longitudinal axis; since the rectangle's area is proportional to that of the seminiferous tubule section, we used the rectangle area to represent the area of the seminiferous tubule section. Statistical significance of cellular composition analysis between the two data groups by Student's t-test (two-tailed) were presented but confirmed also by Welch two sample t-test and non-parametric Wilcoxon rank sum test, which is not dependent on normality or symmetry assumption.

DATA AVAILABILITY STATEMENT

The data that support the findings of this study are available on request from the corresponding author. The data are not publicly available due to privacy or ethical restrictions.

ORCID

Eugene Yujun Xu https://orcid.org/0000-0002-4344-6606

REFERENCES

1. Agarwal A, Mulgund A, Hamada A, Chyatte MR. A unique view on male infertility around the globe. *Reprod Biol Endocrinol.* 2015;13(1):1-9.
2. Cooper TG, Noonan E, Von Eckardstein S, et al. World Health Organization reference values for human semen characteristics. *Hum Reprod Update.* 2010;16(3):231-245.
3. Krausz C. Male infertility: pathogenesis and clinical diagnosis. *Best Pract Res Clin Endocrinol Metab.* 2011;25(2):271-285.
4. Matzuk MM, Lamb DJ. The biology of infertility: research advances and clinical challenges. *Nat Med.* 2008;14(11):1197-1213.
5. Hess RA, De Franca LR. Spermatogenesis and cycle of the seminiferous epithelium. *Mol Mech Spermatogen.* 2009;1:1-15.
6. Ahmed EA, de Rooij DG. Staging of mouse seminiferous tubule cross-sections. *Methods Mol Biol.* 2009;558:263-277. doi:10.1007/978-1-60761-103-5_16
7. Zhang C, Gao L, Xu EY. LncRNA, a new component of expanding RNA-protein regulatory network important for animal sperm development. *Semin Cell Dev Biol.* 2016;59C:110-117. doi:10.1016/j.semcdb.2016.06.013
8. Russell LD, Ettlin RA, Hikim APS, Clegg ED. Histological and histopathological evaluation of the testis. *Int J Androl.* 1993;16:83.
9. McLachlan RI, Rajpert-De Meyts E, Hoei-Hansen C, de Kretser DM, Skakkebaek N. Histological evaluation of the human testis—approaches to optimizing the clinical value of the assessment: mini review. *Hum Reprod.* 2007;22(1):2-16.
10. Hess RA, Chen P. Computer tracking of germ cells in the cycle of the seminiferous epithelium and prediction of changes in cycle duration in animals commonly used in reproductive biology and toxicology. *J Androl.* 1992;13(3):185-190.
11. Fakhrzadeh A, Sporndly-Nees E, Ekstedt E, Holm L, Luengo Hendriks CL. New computerized staging method to analyze mink testicular tissue in environmental research. *Environ Toxicol Chem.* 2017;36(1):156-164. doi:10.1002/etc.3517
12. Creasy DM, Panchal ST, Garg R, Samanta P. Deep learning-based spermatogenic staging assessment for hematoxylin and eosin-stained sections of rat testes. *Toxicol Pathol.* 2021;49(4):872-887. doi:10.1177/0192623320969678
13. Dumont L, Levacher N, Schapman D, et al. IHC_Tool: an open-source Fiji procedure for quantitative evaluation of cross sections of testicular explants. *Reprod Biol.* 2021;21(2):100507.
14. Xu J, Lu H, Li H, et al. Computerized spermatogenesis staging (CSS) of mouse testis sections via quantitative histomorphological analysis. *Med Image Anal.* 2021;70:101835.
15. Yang R, Stendahl AM, Vigh-Conrad KA, Held M, Lima AC, Conrad DF. SATINN: an automated neural network-based classification of testicular sections allows for high-throughput histopathology of mouse mutants. *Bioinformatics.* 2022;38(23):5288-5298.
16. Ito Y, Unagami M, Yamabe F, et al. A method for utilizing automated machine learning for histopathological classification of testis based on Johnsen scores. *Sci Rep.* 2021;11(1):9962. doi:10.1038/s41598-021-89369-z
17. Meikar O, Majoral D, Heikkinen O, et al. STAGETOOL, a novel automated approach for mouse testis histological analysis. *Endocrinology.* 2022;164(2):bqac202. doi:10.1210/endocr/bqac202
18. Liang S, Lu H, Zang M, et al. Deep SED-Net with interactive learning for multiple testicular cell types segmentation and cell composition analysis in mouse seminiferous tubules. *Cytometry Part A.* 2022;101(8):658-674.
19. Lu H, Zang M, Marini GPL, et al. A novel pipeline for computerized mouse spermatogenesis staging. *Bioinformatics.* 2022;38(23):5307-5314.
20. Ghoshal B, Hikmet F, Pineau C, Tucker A, Lindskog C. DeepHistoClass: a novel strategy for confident classification of immunohistochemistry images using deep learning. *Mol Cell Proteomics.* 2021;20:100140.
21. Bell S, Zsom A, Conley J, Spade D. Automated identification of multinucleated germ cells with U-Net. *PLoS ONE.* 2020;15(7):e0229967.
22. Holzinger A. Interactive machine learning for health informatics: when do we need the human-in-the-loop?. *Brain Informatics.* 2016;3(2):119-131.
23. Guo X, Yu Q, Li R, et al. Intelligent medical image grouping through interactive learning. *Int J Data Sci Anal.* 2016;2:95-105.
24. Guo X. *Discovering a Domain Knowledge Representation for Image Grouping: Multimodal Data Modeling, Fusion, and Interactive Learning.* Rochester Institute of Technolog; 2017.
25. Ba W, Wang S, Shang M, et al. Assessment of deep learning assistance for the pathological diagnosis of gastric cancer. *Mod Pathol.* 2022;35(9):1262-1268.
26. Ho DJ, Agaram NP, Schüffler PJ, et al. *Deep Interactive Learning: An Efficient Labeling Approach for Deep Learning-Based Osteosarcoma Treatment Response Assessment.* Springer; 2020:540-549.
27. Goldstrohm AC, Hall TMT, McKenney KM. Post-transcriptional regulatory functions of mammalian Pumilio proteins. *Trends Genet.* 2018;34(12):972-990. doi:10.1016/j.tig.2018.09.006
28. VanGompel MJ, Xu EY. The roles of DAZ gene family in spermatogenesis–more than just translation. *Spermatogenesis.* 2011;1(1):36-46.
29. Li H, Liang Z, Yang J, et al. DAZL is a master translational regulator of murine spermatogenesis. *Natl Sci Rev.* 2019;6:455-468.
30. Mikedis MM, Fan Y, Nicholls PK, et al. DAZL mediates a broad translational program regulating expansion and differentiation of spermatogonial progenitors. *Elife.* 2020;9:e56523. doi:10.7554/eLife.56523
31. Ruggiu M, Speed R, Taggart M, et al. The mouse *Dazla* gene encodes a cytoplasmic protein essential for gametogenesis. *Nature.* 1997;389(6646):73-77.
32. Shah C, Vangompel MJ, Naeem V, et al. Widespread presence of human BOULE homologs among animals and conservation of their ancient reproductive function. *PLoS Genet.* 2010;6(7):e1001022.
33. Zhao T, Xiao T, Cao D, et al. Sertoli cell PUMILIO proteins modulate mouse testis size through translational control of cell cycle regulators. *Biol Reprod.* 2022;107(1):135-147.
34. Wreford NG, Rajendra Kumar T, Matzuk MM, de Kretser DM. Analysis of the testicular phenotype of the follicle-stimulating hormone beta-subunit knockout and the activin type II receptor knockout mice by stereological analysis. *Endocrinology.* 2001;142(7):2916-2920. doi:10.1210/endo.142.7.8230
35. Shah C, Vangompel MJ, Naeem V, et al. Widespread presence of human BOULE homologs among animals and conservation of their ancient reproductive function. *PLoS Genet.* 2010;6(7):e1001022.
36. VanGompel MJ, Xu EY. A novel requirement in mammalian spermatid differentiation for the DAZ-family protein Boule. *Hum Mol Genet.* 2010;19(12):2360-2369. doi:10.1093/hmg/ddq109
37. Hess RA. Quantitative and qualitative characteristics of the stages and transitions in the cycle of the rat seminiferous epithelium: light microscopic observations of perfusion-fixed and plastic-embedded testes. *Biol Reprod.* 1990;43(3):525-542. doi:10.1095/biolreprod43.3.525
38. Nakata H, Wakayama T, Takai Y, Iseki S. Quantitative analysis of the cellular composition in seminiferous tubules in normal and genetically modified infertile mice. *J Histochem Cytochem.* 2015;63(2):99-113.

39. Lecureuil C, Fontaine I, Crepieux P, Guillou F. Sertoli and granulosa cell-specific Cre recombinase activity in transgenic mice. Research support, non-U.S. Gov't. *Genesis*. 2002;33(3):114-118. doi:10.1002/gene.10100

40. Eberhart CG, Maines JZ, Wasserman SA. Meiotic cell cycle requirement for a fly homologue of human Deleted in Azoospermia. *Nature*. 1996;381(6585):783-785.

41. Hess RA, Renato de Franca L. Spermatogenesis and cycle of the seminiferous epithelium. *Adv Exp Med Biol*. 2008;636:1-15. doi:10.1007/978-0-387-09597-4_1

42. Russell LD, Ettlin RA. In: AP Clegg, ed. *Histological and Histopathological Evaluation of the Testis*. Cache River Press; 1990.

43. Griswold MD. The central role of Sertoli cells in spermatogenesis. Review. *Semin Cell Dev Biol*. 1998;9(4):411-416. doi:10.1006/scdb.1998.0203

44. He K, Zhang X, Ren S, Sun J. Deep residual learning for image recognition. Proceedings of the IEEE Conference on Computer Vision and Pattern Recognition, Las Vegas. 2016:770-778.

45. Hu J, Shen L, Sun G. Squeeze-and-excitation networks. 2018 IEEE Conference on Computer Vision and Pattern Recognition, CVPR 2018, Salt Lake City. 2018:7132-7141.

46. Huang G, Liu Z, Van Der Maaten L, Weinberger KQ. Densely connected convolutional networks. Proceedings of the IEEE Conference on Computer Vision and Pattern Recognition, Honolulu. 2017:4700-4708.

47. Woo S, Park J, Lee J-Y, Kweon IS. Cbam: Convolutional block attention module. European Conference on Computer Vision (ECCV), Munich. 2018:3-19.

48. Fraz M, Shaban M, Graham S, Khurram SA, Rajpoot NM. *Uncertainty Driven Pooling Network for Microvessel Segmentation in Routine Histology Images*. Springer; 2018:156-164.

49. Badrinarayanan V, Kendall A, Cipolla R. Segnet: a deep convolutional encoder-decoder architecture for image segmentation. *IEEE Trans Pattern Anal Mach Intell*. 2017;39(12):2481-2495.

50. Ronneberger O, Fischer P, Brox T. *U-Net: Convolutional Networks for Biomedical Image Segmentation*. Springer; 2015:234-241.

51. Zhou Z, Rahman Siddiquee MM, Tajbakhsh N, Liang J. *Unet++: A Nested U-Net Architecture for Medical Image Segmentation*. Springer; 2018:3-11.

52. Oktay O, Schlemper J, Folgoc LL, et al. Attention U-net: learning where to look for the pancreas. arXiv preprint arXiv:180403999. 2018.

SUPPORTING INFORMATION

Additional supporting information can be found online in the Supporting Information section at the end of this article.

How to cite this article: Ao N, Zang M, Lu Y, et al. Rapid detection of mouse spermatogenic defects by testicular cellular composition analysis via enhanced deep learning model. *Andrology*. 2024;1-19. https://doi.org/10.1111/andr.13773